DOI: 10.1002/((please add manuscript number))
Article type: Communication

Exfoliated Mesoporous 2D Covalent Organic Frameworks for High-Rate Electrochemical Double-Layer Capacitors

*Yusran Yusran, Hui Li, Xinyu Guan, Daohao Li, Lingxue Tang, Ming Xue, Zhongbin Zhuang, Yushan Yan, Valentin Valtchev, Shilun Qiu and Qianrong Fang**

Y. Yusran, H. Li, X. Guan, Dr. D. Li, L. Tang, Prof. M. Xue, Prof. S. Qiu, Prof. Q. Fang
State Key Laboratory of Inorganic Synthesis and Preparative Chemistry, Jilin University, Changchun 130012, P. R. China
E-mail: qrfang@jlu.edu.cn

Prof. Z. Zhuang
State Key Lab of Organic-Inorganic Composites and Beijing Advanced Innovation Center for Soft Matter Science and Engineering, Beijing University of Chemical Technology, Beijing 100029, P. R. China

Prof. V. Valtchev
Normandie Univ, ENSICAEN, UNICAEN, CNRS, Laboratoire Catalyse et Spectrochimie, 6 Marechal Juin, 14050 Caen, France

Prof. Y. Yan
Department of Chemical and Biomolecular Engineering, Center for Catalytic Science and Technology, University of Delaware, Newark, DE 19716, USA

Keywords: Covalent organic frameworks, chemical exfoliation, double-layer capacitor, high charge-discharge rate

Abstract: The electrochemical double-layer capacitors (EDLCs) are highly demanded electrical energy storage devices due to their high power density with thousands of cycle life compared with pseudocapacitors and batteries. Herein, we report a series of capacitor cells composed of exfoliated mesoporous 2D covalent organic frameworks (e-COFs) that are able to perform excellent double-layer charge storage. The selected mesoporous 2D COFs possess eclipsed AA layer-stacking mode with 3.4 nm square-like open channels, favorable BET surface areas (up to 1170 m^2/g), and high thermal and chemical stabilities. We further exfoliate the COFs via the facile, scalable and mild chemical exfoliation method to produce thin-layer structure with average thickness of about 22 nm. The e-COF-based capacitor cells achieve high areal capacitance (5.46 mF cm^{-2} at 1,000 mV s^{-1}), high gravimetric power (55 kW kg^{-1}), and relatively low τ_0 value (121 ms). More importantly, they performed nearly an ideal DL charge storage at high charge-discharge rate (up to 30,000 mV s^{-1}) and maintained almost 100% capacitance stability even after 10,000 cycles. This study thus provides insights into the potential utilization of COF materials for EDLCs.

In the field of electrochemical energy storage (EES), electrochemical double-layer capacitors (EDLCs) are highly demanded electrical energy storage devices due to their higher power density with thousands of cycle life compared with pseudocapacitors and batteries.[1] The EDLCs involve rapid adsorption of electrolyte ions onto the electrode-electrolyte interfaces.[2] This charge storage system enables EDLCs to endure high charge-discharge rates and long-life cycles without deteriorating the electrode. Notably, a micro-patterned design, namely microcapacitor, can store and deliver charges at relatively high charge-discharge rate (>1,000 mV s^{-1}), in which it is designed by shortening and aligning the ion diffusion path within graphitic-carbon electrode.[3,4] However, the only way to establish microcapacitor architecture relies on the laser-writing[5] and/or lithography techniques[6] that are complex and costly. Thus, it is highly desired to develop non-graphitic carbon capacitors with high charge-discharge rate performance.

Covalent organic frameworks (COFs) are a fascinating class of crystalline porous polymers, where their organic building units are precisely integrated into an extended structure with periodical skeleton and ordered pores.[7] The synthesis of COFs follows the reticular chemistry principle, which provides judicious control of two- or three-dimensional networks, porosity and physicochemical properties (stability, optical, conductivities and so on).[8] Specifically, 2D COFs generally possess eclipsed-layer stacking with typical 1D-aligned perpendicular channel mimicking the structural backbone of graphene.[9] This structural feature provides an aligned diffusion pathway for ions or charges mobility and ensures efficient mass transport. In fact, 2D COFs have been extensively studied for proton[10] electrical[11] conductionand as charge carriers.[12] The results show that the 2D COFs with high surface areas are attractive for EES applications, especially for EDLC electrode construction. In the previous attempts, several 2D COFs have been tested as active materials

for pseudocapacitor electrode construction. For instance, Dichtel *et al.* mixed DAAQ-TFP COF (35 wt%) and carbon black (60 wt%) to fabricate pseudocapacitor electrode for the first time,[13] while Jiang *et al.* utilized NiP-COF (20 wt%) to do so.[14] Furthermore, other 2D COFs have been designed and utilized for similar missions.[15] However, COF-based EDLCs have rarely been explored so far.

Herein, we prepared EDLC electrodes composed of exfoliated mesoporous 2D COFs (e-COFs) with a pore size of 3.4 nm and high specific surface areas. These capacitor cells performed nearly an ideal DL charge storage at high charge-discharge rate (up to 30,000 mV s^{-1}), and achieved high areal capacitance (5.46 mF cm^{-2} at 1,000 mVs^{-1}), relatively low τ_0 value (121 ms) and high gravimetric power (55 kW kg^{-1}). In addition, they also maintained almost 100% capacitance stability even after 10,000 cycles. To the best of our knowledge, this is the first example of COF-based EDLCs that can demonstrate DL charge storage at high scan rate with superior areal capacitance and gravimetric power.

We designed mesoporous 2D COF series with high surface areas (termed as JUC-510, JUC-511, and JUC-512; JUC = Jilin University China) and further exfoliated them to obtain few-layer COFs for fabricating EDLC electrodes (Figure 1). These COFs were synthesized by employing a linear building block of hydroxyl containing 4,4'-(1,2-ethynediyl)bis-2-hydroxybenzaldehyde (**1**) as the basic backbone (Figure 1a).[16] Condensing (**1**) with the square-shape 5,10,15,20-tetrakis[(4-aminophenyl)porphyrin (**2**) into an anhydrous ethanol/*o*-dichlorobenzene mixed solvent, the crystalline solid of JUC-510 was produced with a high yield (85%). Meanwhile, by using 5,10,15,20-tetrakis[(4-aminophenyl)porphyrinato]nickel(II) (**3**) or 5,10,15,20-tetrakis[(4-aminophenyl)porphyrinato]copper(II) (**4**), both JUC-511 and JUC-512 were exclusively obtained with very convincing yields (~ 83%). The advantages of utilizing building block (**1**) can not only drive the formation of large pores but also possibly establish hydrogen bonding within the framework of targeted COFs, which has been reported to enhance the chemical stability of COFs to high extent.[17]

The successful condensation among the building blocks was systematically studied by Fourier-transform infrared (FT-IR) and solid-state ^{13}C cross-polarization magic angle spinning (CP-MAS) NMR spectroscopies. The new stretching band emerged at 1590 cm^{-1} on the FT-IR spectrum of JUC-510 corresponds to the formation of imine (-C=N-) linkages (Figure S1, Supporting Information). This result was concomitant with the significant diminishment of stretching band at 1665 cm^{-1} assignable to the absorption band for carbonyl (C=O) group of (**1**) and at 3370 cm^{-1} corresponding to the stretching band of amine group of (**2**). A similar phenomenon was observed on the FT-IR spectra of both JUC-511 and JUC-512, in which the establishment of imine linkages was recorded at 1589 cm^{-1} and 1586 cm^{-1}, respectively (Figures S2 and S3, Supporting Information). Meanwhile, the solid-state ^{13}C CP-MAS NMR spectroscopy further confirmed the formation of carbon-nitrogen species in JUC-510, 511, and 512, where clear resonance signals at δ = 160 ppm corresponding to the carbon atom of the imine linkage were observed (Figures S4-6, Supporting Information). The crystal morphology was examined by scanning electron microscopy (SEM, Figures S23-25, Supporting Information) and transmission electron microscopy (TEM, Figure 2d; Figures S26-28, Supporting Information), which showed isometric crystals with highly aggregated rod-like morphology.

The crystallinity and unit cell parameters of COFs were resolved by powder X-ray diffraction (PXRD) analysis and further corroborated with the structural simulation using Materials Studio software package (version 7.0).[18] The structural models of COFs after a geometrical energy minimization reveal that they adopt P_4 space group with unit cell parameters of $a = b = 45.95$ Å, $c = 3.65$ Å and $\alpha = \beta = \gamma = 90°$ for JUC-510; $a = b = 45.91$ Å, $c = 3.66$ Å and $\alpha = \beta = \gamma = 90°$ for JUC-511; and $a = b = 45.60$ Å, $c = 3.71$ Å and $\alpha = \beta = \gamma = 90°$ for JUC-512, respectively. The PXRD patterns of the isolated COFs are in good agreement with the simulated patterns as further proved by full profile pattern matching (Pawley) refinements (Figure 2a; Figures S7a and S8a, Supporting Information). The intense

diffraction peak at $2\theta = 2.76°$ corresponds to (110) Bragg peak and additional moderate peaks at $2\theta = 3.90°$, 5.82° and 8.21° are assignable to (200), (300) and (330) Bragg peaks, respectively. Meanwhile, the broad peaks observed at $2\theta > 20°$ (corresponding to (001) Bragg peak) indicate the formation of layered structure strengthened by intralayer π-π interactions. These refinement results offer unit cell parameters that are very close to the prediction with ideal agreement factors ($R_{\omega p}$ = 1.29% and R_p = 0.29% for JUC-510; $R_{\omega p}$ = 2.10% and R_p = 1.39% for JUC-511; and $R_{\omega p}$ = 1.59% and R_p = 1.02% for JUC-512, respectively). Indeed, these structural simulations further confirm that all COFs possess eclipsed AA layer-stacking mode with 3.3 nm predicted 1D square-like open channel (Figure 2b; Figures S7b, S8b and Tables S4-6, Supporting Information). We also anticipated another alternative space group (I_4/m) for their structural models in which the proposed structures are in staggered AB layer-stacking arrangement and the unit of adjacent sheets are horizontally offset by a distance of a/2 and b/2 (Figures S9–11 and Tables S7-9, Supporting Information). However, the PXRD profiles between the simulated and experimental patterns are not matched. On the basis of these results, the COFs are proposed as eclipsed-layer architectures with aligned mesoporous pores. We assume that the tendency of forming eclipsed layer stacking COFs is due to the presence of hydrogen bonding effects and the π-π interactions between the adjacent sheets. Furthermore, the COFs are optic-active materials under solid-state UV-Vis spectroscopy (Figures S12–14, Supporting Information). JUC-511 absorbs a wide range of visible light (λ = 400–750 nm) with maximum adsorption at λ = 445 nm, 550 nm and 600 nm. Essentially, it exhibits broad Soret band centered at λ = 445 nm which is red-shifted 5 nm relative to (**3**), indicating the present of conjugated structure. The similar red-shifted phenomenon is observed in JUC-512 and JUC-510 samples, confirming the presence of similar conjugated structures in both COFs.

The porosity of COFs was evaluated by nitrogen (N_2) adsorption-desorption measurement at 77 K (Figure 2c; Figures S15 and S16, Supporting Information). For

example, the adsorption isotherm of JUC-511 belongs to typical type-IV isotherm, indicating the mesoporous character. Specifically, the sharp increase of N_2 uptake amount at low pressure (P/P_0 < 0.05) indicates that the N_2 molecules feeding into the square-like pores rapidly. Meanwhile, the isotherm's inclination between P/P_0 = 0.2 and 0.4 is observed, which further confirms the presence of textural mesopores. The Brunauer-Emmett-Teller (BET) surface area of JUC-511 is about 842 m^2/g. Meanwhile, the pore size distribution based on the non-local density functional theory (NL-DFT) confirms the presence of 3.4 nm open channel, which is very close with the predicted structure (3.3 nm). Furthermore, both JUC-510 and JUC-512 exhibit similar porosity character (BET surface area of 1170 m^2/g and pore size of 3.4 nm for JUC-510 as well as BET surface area of 704 m^2/g and pore size of 3.4 nm for JUC-512). JUC-510 achieves slightly higher BET surface area due to the absence of metal species on porphyrin moiety of JUC-510. The total pore volume determined at P/P_0 = 0.9 is 0.80 cm^3/g, 0.71 cm^3/g and 0.54 cm^3/g for JUC-510, JUC-511 and JUC-512, respectively.

It is known that the stability of active materials is an essential issue for EDLC electrodes; hence these COFs' stabilities were further studied. Notably, the isolated COFs were chemically stable in common organic solvents (THF, MeOH, hexane, acetonitrile, acetone, and DMF for 24 h) and water (at 25 °C, 24 h). Furthermore, they maintained structural integrity in both 1 N HCl and 1 N NaOH at 25 °C overnight (Figures S17–19, Supporting Information). This remarkable structural stability may originate from the presence of intralayer hydrogen bonding, which interlocks the tetragonal 2D sheets in planar conformation.[19] Besides, the AA layer-stacking mode further amplifies the interaction to enhance structural integrity. On the other hand, the COFs exhibit high thermal stability up to 380 °C under thermal gravimetric analysis (TGA) (Figures S20–22, Supporting Information).

We further exfoliated above COFs via the facile, scalable and mild chemical exfoliation method to produce e-COFsOur approach is milder than the ball-milling method,[20] and it is able to to exfoliate the 2D COF thus providing the required thin sheets, which are

indispensible to reach high capacitance and relatively low τ_0 values. The SEM images of e-COFs display fined-layer like morphologies, which fundamentally contrast with their parent COFs (Figures S28–30, Supporting Information). Furthermore, the atomic force microscopy (AFM) analysis reveals that e-COFs establish thin-layer structure with average thickness of ~ 22 nm (Figure 3a; Figures S31-33, Supporting Information). On the contrary, their parent COFs possess typical aggregate particles and are much thicker (215–389 nm). TEM images of e-COFs shown typical exfoliated layer-like structures which corroborate with their SEM images (Figure 3b; Figures S34 and S35, Supporting Information). Since COFs are electron-beam sensitive materials, it is challenging to obtain the diffraction pattern under selective area electron diffraction (SAED)-TEM method. However, additional live-FFT capture of certain areas of e-COFs confirms the presence of ordered lattice. Furthermore, their PXRD patterns reveal the preservation of the major peaks relative to pristine COFs (Figure 3c; Figures S36 and S37, Supporting Information).

The surface area reduction was clearly seen on e-COFs samples (Figures S38–40, Supporting Information). For instance, e-JUC-511 exhibits a BET surface area of 416.6 m^2/g, which is 50% lower than that of pristine JUC-511. Meanwhile, both e-JUC-512 and e-JUC-510 manage a BET surface area of 336 m^2/g and 666 m^2/g, respectively. Indeed, those surface areas are much higher than many other reported covalent organic nanosheets (CONs).[21] In addition, the pore size of e-COFs remains essentially unchanged relative to their parent COFs. All these results mentioned above indicate that the exfoliation treatment does not lead to serious structural deformation. In addition, e-COFs demonstrate notable thermal stability up to 350 °C (Figures S41–43, Supporting Information). Due to their high surface area and defined layer-structure with spacious pore size, e-COFs are promising materials for EDLC electrode.

In the prior analysis, CV tests were performed on both COF and e-COF capacitor cells in the full 1.3 V working potential window to access their charge storage behaviour (Figures

S44–46, Supporting Information). The CV curves of e-COF capacitor cells exhibited almost ideal rectangular curves when cycled at a scan rate of 50 mV s^{-1}. These voltammogram features indicated the DL charge storage took place. In addition, no noticeable redox waves were observed, confirming that the DL charge storage was dominant over possible Faradic-storage. In contrast, the CV curves of COF capacitor cells demonstrated typical distorted rectangular shape when cycled at similar working potential window and scan rate. Their voltammograms features revealed the sluggish ion adsorption and inefficient charge storage. These results emphazise that layer exfolation enables DL charge storage and allows for fast ion transport. We assume that it enhances the accessible surface area for charge occupation and shortens the ion diffusion path (Figure 1b). To prove this assumption, we further performed CV tests on e-COF capacitor cells at higher scan rate (100–1,000 mV s^{-1}). Notably, retained rectangular voltammogram was demonstrated even at 1,000 mV s^{-1}, which reveals the high charge-discharge rate capability of e-COF capacitor cells (Figure 3d; Figure S47, Supporting Information). It is worth noting that this rate capability is rarely reported among conventional graphitic-carbon capacitors and other reported COF-based capacitors (commonly operated at scan rate of ≤ 100–500 mV s^{-1}).

We further performed CV tests on e-COF capacitor cells at higher scan rates (3,000–10,000 mV s^{-1}) to evaluate their rate capabilities and charge storage stabilities (Figure 4a–b). Remarkably, the CV profiles of both e-JUC-511 and e-JUC-512 capacitor cells can retain rectangular voltammograms. These CV results reveal the significantly high rate capabilities and charge storage stablities of both capacitor cells in delivering and storing charges simultaneously. Noteworthy, this performance is maintained even at high scan rate (up to 30,000 mV s^{-1}), which is two orders of magnitude higher than CV of conventional graphitic-carbon capacitors and comparable with microcapacitors (Figures S48 and S49, Supporting Information). The ability to store charges at high charge-dischage rate implies the fully accesbile surface area and the efficient mobility of the charges and ions within the entire

electrode. Meanwhile, e-JUC-510 capacitor cell can also be cycled up to 7,000 mV s^{-1}, which is relatively lower rate performance compared to those of e-JUC-511 and e-JUC-512 capacitor cells. However, it is still relatively significant compared to conventional graphitic-carbon capacitors (Figure S50, Supporting Information). This result is fairly reasonable since both e-JUC-511 and e-JUC-512 contain electroactive metal (Ni and Cu), which enhance the ionic conductivity of corresponding e-COFs and the possible faradic-storage contribution. The redox peaks are not apparent on their CV curves, clarifying that DL storage dominates the storage mechanism. Since e-COF capacitor cells contained a minor amount of carbon-black as conductive agent (having microporous pore), CV test was further performed on conductive carbon capacitor cell to analize its contribution to the high rate performance of e-COF capacitor cells (Figure S51, Supporting Information). As clearly seen, this capacitor cell could only perform efficient DLs charge storage at low scan rate (100 mV s^{-1}) and started to diminish at more higher scan rate (500–1,000 mV s^{-1}). Once again, this result clearly emphasizes the high rate capability and efficient DL charge storage in e-COF capacitor cells.

Indeed, the ability to sustain at a high rate is representative of high instantaneous power corresponding to high specific capacitance.[3] Notably, both e-JUC-511 and e-JUC-512 capacitor cells manage a high areal capacitance of 5.46 mF cm^{-2} and 5.85 mF cm^{-2} at 1,000 mVs^{-1}, respectively. Meanwhile, e-JUC-510 capacitor cell achieves areal capacitance of 4.17 mF cm^{-2} at similar scan rate (Table S1). Comparatively, those values are three-times higher than that from the state-of-the-art onion-like carbon (OLC) microcapacitor (1.7 mF cm^{-2} at 1,000 mVs^{-1}),[3] much higher than other graphitic carbon micro-patterned capacitors (at a scan rate of 1–100 mVs^{-1}) and laser-scribed graphene based capacitor (3.67 mF cm^{-2}, Table S2).[22] Considering their simple fabrication technique (without micro-patterned approach) and high charge-discharge rate capability, the areal capacitances of e-COF capacitor cells are superior to graphitic-carbon microcapacitors. Furthermore, as the manifestation of their high rate performance, both e-JUC-511 and e-JUC-512 capacitor cells show significant maximum

power density (P_{max}, per volummetric stack device) compared to several graphitic-carbon microcapacitors. For instance, power densities of 5.32 W cm^{-3} and 4.08 W cm^{-3} are successfully achieved by e-JUC-511 and e-JUC-512 capacitor cells, respectively. Again, those values are much higher than those of OLC microcapacitors (~ 1.0 W cm^{-3}) and hydrated GO microcapacitors (1.7 W cm^{-3}). Meanwhile, they also show moderate energy (E_{max}, per volummetric stack device) of ~ 0.26 mWh cm^{-3}. Furthermore, considering the mass of the active material, both e-JUC-511 and e-JUC-512 capacitor cells manifest maximum gravimetric power (P_{gra}) of 55.0 kW kg^{-1} and 42.2 kW kg^{-1}, respectively. It is an exciting result that their gravimetrric powers are superior to graphitic-carbon based capacitors, including curved-graphene capacitors, nitrogen-doped mesoporous carbon capacitors and reduced graphene-oxide (rGO) capacitors (Table S3). Nevertheless, up to 50% of the areal capacitances is maintained by both capacitor cells, even at high scan rate (10,000 mV s^{-1}, Table S1). On the other hand, e-JUC-510 capacitor cell manages maximum power density of 1.02 W cm^{-3}, energy density of 0.23 mWh cm^{-3}, and gravimetric power of 9.93 kW kg^{-1}, respectively.

To further analyze the high rate capability of e-COF capacitor cells, the electrochemical impedance spectroscopy (EIS) method was applied. The analysis is conducted at a frequency range of 10 mHz–10 kHz with amplitude of 10 mV (Figure 4c–d; Figure S52, Supporting Information). The Nyquist plots of both e-JUC-511 and e-JUC-512 capacitor cells exhibit pure capacitive behavior even at high frequencies (0.38 kHz for e-JUC-511 and 0.32 kHz for e-JUC-512 capacitor cells, respectively). The results indicate the efficient charge mobility within the entire electrodes of both cells (Figure 4c). Nevertheless, they demonstrate small equivalent series resistance (ESR, obtained from the intercept of the real axis) of 10.8 Ω for e-JUC-511 and 15.5 Ω for e-JUC-512 capacitor cells. These small ESR values mean the excellent ionic conductivity and very low internal electrolyte-electrode resistance within the electrodes. Indeed, they also prove the efficient ion propagation and efficient formation of DL

charge storage within electrodes of both cells. The high charge-dicharge rate performance of both capacitor cells can be attributed to the small ESR values. Interestingly, e-JUC-510 capacitor cell exhibits a little higher ESR value (60 Ω) with relatively lower capacitance response (detected at frequency of 68 Hz), exemplifying that the presence of electroactive metal plays the pivotal role in enhancing the ionic conductivity of the electrodes (Figure S52a, Supporting Information). Furthermore, the Bode plots of e-COF capacitor cells further amplify their high charge-dicharge rate performance (Figure 4d). Notably, both e-JUC-511 and e-JUC-512 capacitor cells exhibit high characteristic frequency constants (f_o, obtained at -phase = 45^o) of 8.25 Hz and 5.62 Hz respectively, which indicates the fast and robust ion transport within the electrodes. Depending on these values, the relaxation time constants (τ_0, a minimum time needed to discharge all the energy from electrode with an efficiency more than 50%)[3] are further determined. Remarkably, the τ_0 value is about 121 ms for e-JUC-511 and 178 ms for e-JUC-512, which represents the fast discharging process. Significantly, those τ_0 values are much lower than those of reported activated carbon microcapacitor (700 ms) and chemically reduced graphene oxide capacitor (188 ms).[3,24] Meanwhile, e-JUC-510 capacitor cell exhibits capacitive response of 68 Hz with relatively high τ_0 value (464 ms) (Figure S52b, Supporting Information). Nevertheless, those small τ_0 values further emphasize the high charge-discharge rate and superior capacitive response in e-COF capacitor cells.

The galvanostatic charge-discharge (GCD) method is also employed to explore the charge-discharge behaviors of e-COF capacitor cells. Interestingly, e-COF capacitor cells demonstrate an efficient charge-discharge process within second domain of time (Figures S53–55, Supporting Information). Specifically, they exhibit nearly ideal triangular curves without obvious voltage drop, indicating the simultaneous and rapid charge-discharge within each electrode over potential applied. This result further reveals the effcient charge storage and fast ion adsorption behaviors within e-COF capacitor cells, which is much faster than batteries, conventional capacitors and in-line with those of microcapacitors. In brief, the CV,

EIS and GCD analyses provide clear evidence of the high charge-discharge rate and superior capacitive performance of e-COF capacitor cells. These results, however, corroborate that layer exfoliation method provides fast ion mobility by providing shorter ion transport path within the entire active surface of the electrodes. Thus, it allows for efficient DL charge storage and enhances power performance.

From the commercial and industrial point of view, the robustness of the capacitor cell is a crucial aspect. The stability and reliability issues are essential parameters for electrical energy storage materials. In view of these characteristics, the stability and reliability of both e-JUC-511 and e-JUC-512 capacitor cells were evaluated due to their significant power performance (Figure 5; Figures S56 and S57, Supporting Information). Notably, both e-JUC-511 and e-JUC-512 capacitor cells maintained nearly 100% capacitance retention even after 10,000 consecutive cycles (Figure 5a). In consideration of practical applications, capacitors are usually assembled either in parallel or series configurations to reach certain operating voltage or output current. The adaptability of e-COF capacitor cells for serial and parallel configurations was demonstrated by connecting three coins (packaged in alligator clip, Figure 5b-e; Figures S56 and S57, Supporting Information). As clearly depicted, the tandem cells exhibited good control over the operating voltage window and capacity when the voltage range was increased in parallel of series combination. Essentially, in both configurations, e-COF capacitor cells established almost ideal rectangular in shape voltammograms and triangular charge-discharge curves without significant voltage drop, which again proves the robust and reliability of e-COF capacitor cells. All these results reveal the reliable performance of e-COF capacitor cells as prospective EES material.

In addition, the capacitive performances of e-COF capacitor cells were compared with other energy-storage devices (commercial battery and capacitor) presented in the Ragone plot (Figure 6). The plot presents the power and energy densities of all devices being compared. To this comparison, both power and energy densities of e-COF capacitor cells were calculated

based on the volummetric stack of the assembled coin-cell, including the micron thickness of the active electrode, current collector and separator as well. Notably, e-COF capacitor cells exhibited maximum power density of 4.1-5.4 W cm^{-3}, which are two-order of magnitude higher than Li thin-film battery, one-order of magnitude higher than commercial activated carbon and comparable with Al electrolytic capacitor. Meanwhile, they showed a moderate maximum energy density (~ 0.27 mWh cm^{-3}), which is two-order of magnitude higher than Al electrolytic capacitor and comparable with activated carbon electrochemical capacitor. Indeed, this plot placed e-COF capacitor cells as potential power supply. Finally, we expected that the energy and power densities could be potentially increased with improved processing and device optimization by extending the working potential window. Based on these promissing results, optimization studies will be performed in order to further improve the electrochemical double-layer capacitator performance.

In summary, we have demonstrated that COFs, as highly crystalline and porous materials are prospective active candidates for construction EDLCs. We prepared capacitor cells composed of exfoliated 2D mesoporous COFs, which showed an ideal DL charge storage and high charge-discharge rate, a rare phenomenon in conventional graphitic-carbon and COFs-based capacitors. Moreover, compared to graphitic-carbon microcapacitors and conventional capacitors, they exhibited superior areal capacitance (5.46 mF cm^{-2} at 1,000 mV s^{-1}) and gravimetric power (55 kW kg^{-1}). Indeed, these preliminary results could provide an early view for further researches in employing COFs as potential active materials for ELDC electrodes. We also forecast that COFs hold great promise for microcapacitors that we expect to show more sophisticated performance.

Supporting Information

Supporting Information is available from the Wiley Online Library or from the author.

Acknowledgements

This work was supported by National Natural Science Foundation of China (21571079, 21621001, 21390394, 21571076, and 21571078), ″111″ project (B07016 and B17020), and the program for JLU Science and Technology Innovative Research Team. V.V. and Q.F. acknowledge the Thousand Talents program (China). V.V., S.Q. and Q.F. acknowledge funding from the French-Sino International Laboratory (LIA) ″Zeolites″.

Received: ((will be filled in by the editorial staff))
Revised: ((will be filled in by the editorial staff))
Published online: ((will be filled in by the editorial staff))

References

[1] a) P. Simon, Y. Gogotsi, *Nat. Mater.* **2008**, *7*, 845; b) P. Sharma, T. S. Bhatti, *Energy Convers. Manag.* **2010**, *51*, 2901; c) Y. Wang, Y. Song, Y. Xia, *Chem. Soc. Rev.* **2016**, *45*, 5925.

[2] F. Wang, X. Wu, X. Yuan, Z. Liu, Y. Zhang, L. Fu, Y. Zhu, Q. Zhou, Y. Wu, W. Huang, *Chem. Soc. Rev.* **2017**, *46*, 6816.

[3] D. Pech, M. Brunet, H. Durou, P. Huang, V. Mochalin, Y. Gogotsi, P. -L. Taberna, P. Simon, *Nat. Nanotechnol.* **2010**, *5*, 651.

[4] W. Gao, N. Singh, L. Song, Z. Liu, A. L. M. Reddy, L. Ci, R. Vajtai, Q. Zhang, B. Wei, P. M. Ajayan, *Nat. Nanotechnol.* **2011**, *6*, 496.

[5] M. F. El-Kady, R. B. Kaner, *Nat. Commun.* **2013**, *4*, 1475.

[6] a) Z. S. Wu, K. Parvez, X. Feng, K. Müllen, *Nat. Commun.* **2013**, *4*, 2487; b) M. Beidaghi, C. Wang, *Adv. Funct. Mater.* **2012**, *22*, 4501.

[7] a) C. S. Diercks, O. M. Yaghi, *Science* **2017**, *355*, eaal1585; b) N. Huang, P. Wang, D. Jiang, *Nat. Rev. Mater.* **2016**, *1*, 16068; c) S.-Y. Ding, W. Wang, *Chem. Soc. Rev.* **2013**, *42*, 548; d) J. W. Colson, W. R. Dichtel, *Nat. Chem.* **2013**, *5*, 453.

[8] a) N. W. Ockwig, A. P. Côté, M. O'Keeffe, A. J. Matzger, O. M. Yaghi, *Science* **2005**, *310*, 1166; b) P. Kuhn, M. Antonietti, A. Thomas, *Angew. Chem. Int. Ed.* **2008,** *47,*

3450; c) O. M. Yaghi, *J. Am. Chem. Soc.* **2016**, *138*, 15507; d) P. J. Waller, F. Gándara, O. M. Yaghi, *Acc. Chem. Res.* **2015**, *48*, 3053; e) X. Y. Guan, Y. C. Ma, H. Li, Y. Yusran, M. Xue, Q. R. Fang, Y. S. Yan, V. Valtchev, S. L. Qiu, *J. Am. Chem. Soc.* **2018**, *140*, **4494; f)** S. C. Yan, X. Y. Guan, H. Li, D. H. Li, M. Xue, Y. S. Yan, V. Valtchev, S. L. Qiu, Q. R. Fang, *J. Am. Chem. Soc.* **2019**, *141*, **2920**.

[9] a) X. Feng, X. Ding, D. Jiang, *Chem. Soc. Rev.* **2012**, *41*, 6010; b) Q. R. Fang, Z. B. Zhuang, S. Gu, R. B. Kaspar, J. Zheng, J. H. Wang, S. L. Qiu, Y. S. Yan, *Nat. Commun.* **2014**, *5*, 4503; c) Y. Peng, Z. Hu, Y. Gao, D. Yuan, Z. Kang, Y. Qian, N. Yan, D. Zhao, *ChemSusChem* **2015**, *8*, 3208; d) Q. Sun, B. Aguila, J. A. Perman, N. T.-K. Nguyen, S. Q. Ma, *J. Am. Chem. Soc.* **2016**, *138*, 15790; e) X. Y. Guan, H. Li, Y. C. Ma, M. Xue, Q. R. Fang, Y. S. Yan, V. Valtchev, S. L. Qiu, *Nat. Chem.* **2019**, *11*, 587.

[10] a) Q. Xu, S. Tao, Q. Jiang, D. Jiang, *J. Am. Chem. Soc.* **2018**, *140*, 7429; b) H. Xu, S. Tao, D. Jiang, *Nat. Mater.* **2016**, *15*, 722.

[11] a) S. Duhović, M. Dincă, *Chem. Mater.* **2015**, *27*, 5487; b) L. Chen, K. Furukawa, J. Gao, A. Nagai, T. Nakamura, Y. Dong, D. Jiang, *J. Am. Chem. Soc.* **2014**, *136*, 9806; c) M. Dogru, M. Handloser, F. Auras, T. Kunz, D. Medina, A. Hartschuh, P. Knochel, T. Bein, *Angew. Chem. Int. Ed.* **2013**, *52*, 2920; d) H. Li, J. H. Chang, S. S. Li, X. Y. Guan, D. H. Li, C. Y. Li, L. X. Tang, M. Xue, Y. S. Yan, V. Valtchev, S. L. Qiu, Q. R. Fang, *J. Am. Chem. Soc.* **2019**, *141*, 13324.

[12] a) X. Ding, L. Liu, Y. Honsho, A. Saeki, S. Seki, S. Irle, Y. Dong, A. Nagai, D. Jiang, *J. Am. Chem. Soc.* **2011**, *133*, 14510; b) S. Wan, F. Gándara, A. Asano, H. Furukawa, A. Saeki, S. K. Dey, L. Liao, M. W. Ambrogio, Y. Y. Botros, X. Duan, S. Seki, J. F. Stoddart, O. M. Yaghi, *Chem. Mater.* **2011**, *23*, 4094; c) S. Jin, K. Furukawa, M. Addicoat, L. Chen, S. Takahashi, S. Irle, T. Nakamura, D. Jiang, *Chem. Sci.* **2013**, *4*, 4505; d) S. Jin, X. Ding, X. Feng, M. Supur, K. Furukawa, S. Takahashi, M. Addicoat, M. E. El-Khouly, T. Nakamura, S. Irle, S. Fukuzumi, A. Nagai, D. Jiang, *Angew.*

Chem. Int. Ed. **2013**, *52*, 2017.

[13] C. R. Deblase, K. E. Silberstein, T. T. Truong, H. D. Abruña, W. R. Dichtel, *J. Am. Chem. Soc.* **2013**, *135*, 16821.

[14] F. Xu, H. Xu, X. Chen, D. Wu, Y. Wu, H. Liu, C. Gu, R. Fu, D. Jiang, *Angew. Chem. Int. Ed.* **2015**, *54*, 6814.

[15] a) S. Chandra, D. R. Chowdhury, M. Addicoat, T. Heine, A. Paul, R. Banerjee, *Chem. Mater.* **2017**, *29*, 2074; b) A. Halder, M. Ghosh, A. M. Khayum, S. Bera, M. Addicoat, H. S. Sasmal, S. Karak, S. Kurungot, R. Banerjee, *J. Am. Chem. Soc.* **2018**, *140*, 10941.

[16] C. Ma, A. Lo, A. Abdolmaleki, M. J. Maclachlan, *Org. Lett.* **2004**, *6*, 3841.

[17] a) X. Chen, M. Addicoat, E. Jin, L. Zhai, H. Xu, N. Huang, Z. Guo, L. Liu, S. Irle, D. Jiang, *J. Am. Chem. Soc.* **2015**, *137*, 3241; b) S. Kandambeth, A. Mallick, B. Lukose, T. Heine, R. Banerjee, *J. Am. Chem. Soc*. **2012**, *134*, 19524.

[18] Materials Studio ver. 7.0, Accelrys Inc., San Diego, CA.

[19] S. Kandambeth, D. B. Shinde, M. K. Panda, B. Lukose, T. Heine, R. Banerjee, *Angew. Chem. Int. Ed.* **2013**, *52*, 13052.

[20] S. Wang, Q. Wang, P. Shao, Y. Han, X. Gao, L. Ma, S. Yuan, X. Ma, J. Zhou, X. Feng, B. Wang, *J. Am. Chem. Soc*. **2017**, *139*, 4258.

[21] a) H. Chen, H. Tu, C. Hu, Y. Liu, D. Dong, Y. Sun, Y. Dai, S. Wang, H. Qian, Z. Lin, L. Chen, *J. Am. Chem. Soc*. **2018**, *140*, 896; b) Y. Peng, Y. Huang, Y. Zhu, B. Chen, L. Wang, Z. Lai, Z. Zhang, M. Zhao, C. Tan, N. Yang, F. Shao, Y. Han, H. Zhang, *J. Am. Chem. Soc*. **2017**, *139*, 8698; c) M. A. Khayum, S. Kandambeth, S. Mitra, S. B. Nair, A. Das, S. S. Nagane, R. Mukherjee, R. Banerjee, *Angew. Chem. Int. Ed.* **2016**, *55*, 15604; d) G. Das, B. P. Biswal, S. Kandambeth, V. Venkatesh, G. Kaur, M. Addicoat, T. Heine, S. Verma, R. Banerjee, *Chem. Sci.* **2015**, *6*, 3931; e) S. Chandra, S. Kandambeth, B. P. Biswal, B. Lukose, M. Kunjir, M. Chaudhary, R. Babarao, T. Heine, R. Banerjee, *J. Am. Chem. Soc*. **2013**, *135*, 17853.

[22] M. F. El-Kady, V. Strong, S. Dubin, R. B. Kaner, *Science* **2012**, *335*, 1326.

[23] A. Eftekhari, *J. Mater. Chem. A* **2018**, *6*, 2866.

[24] P. K. Jha, S. K. Singh, V. Kumar, S. Rana, S. Kurungot, N. Ballav, *Chem.* **2017**, *3*, 846.

Figures

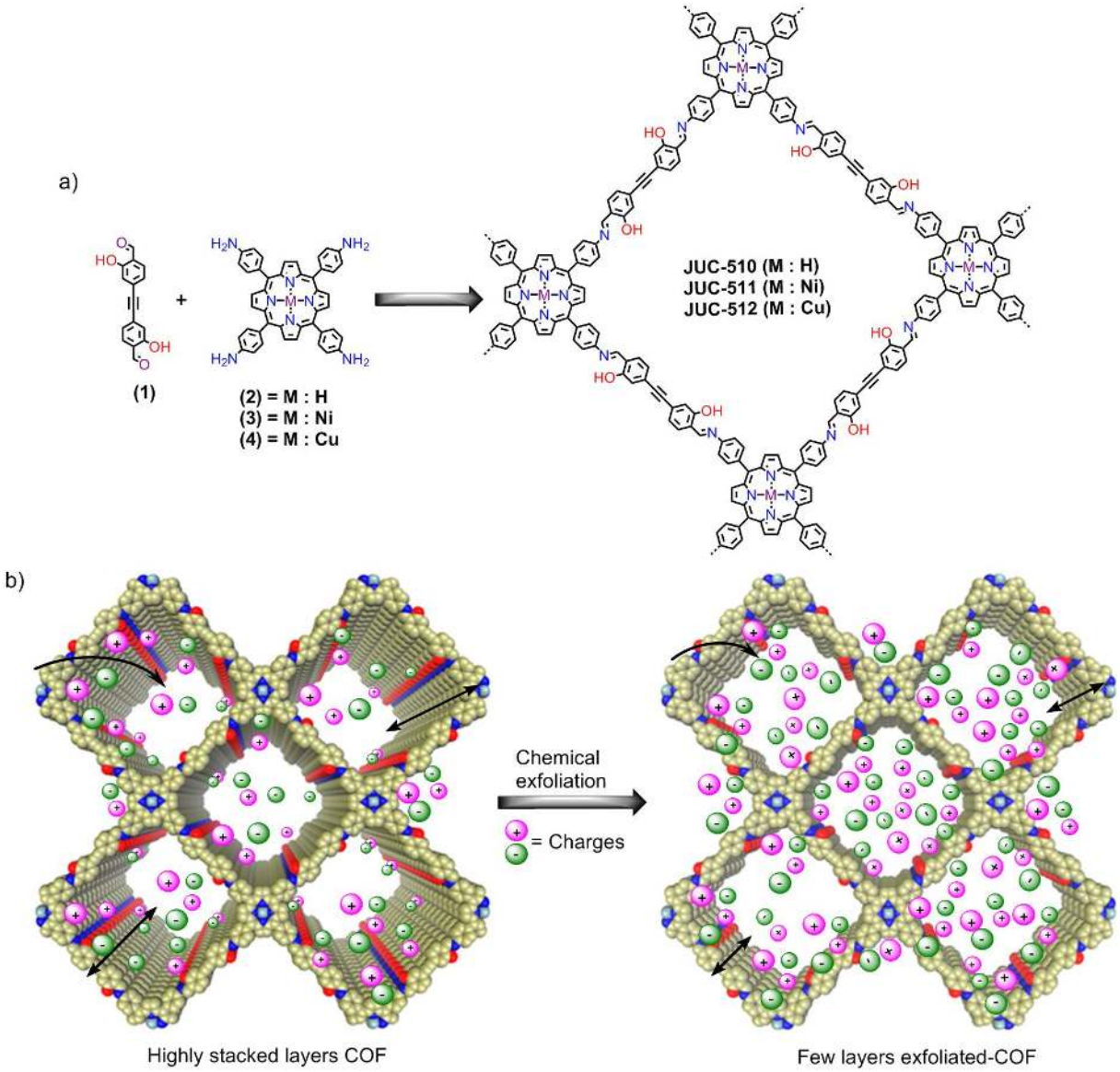

Figure 1. a) Design synthesis of COFs series (JUC-510, JUC-511, and JUC-512); and b) representative diagram of charge storage behavior between COFs and exfoliated COFs (e-COF).

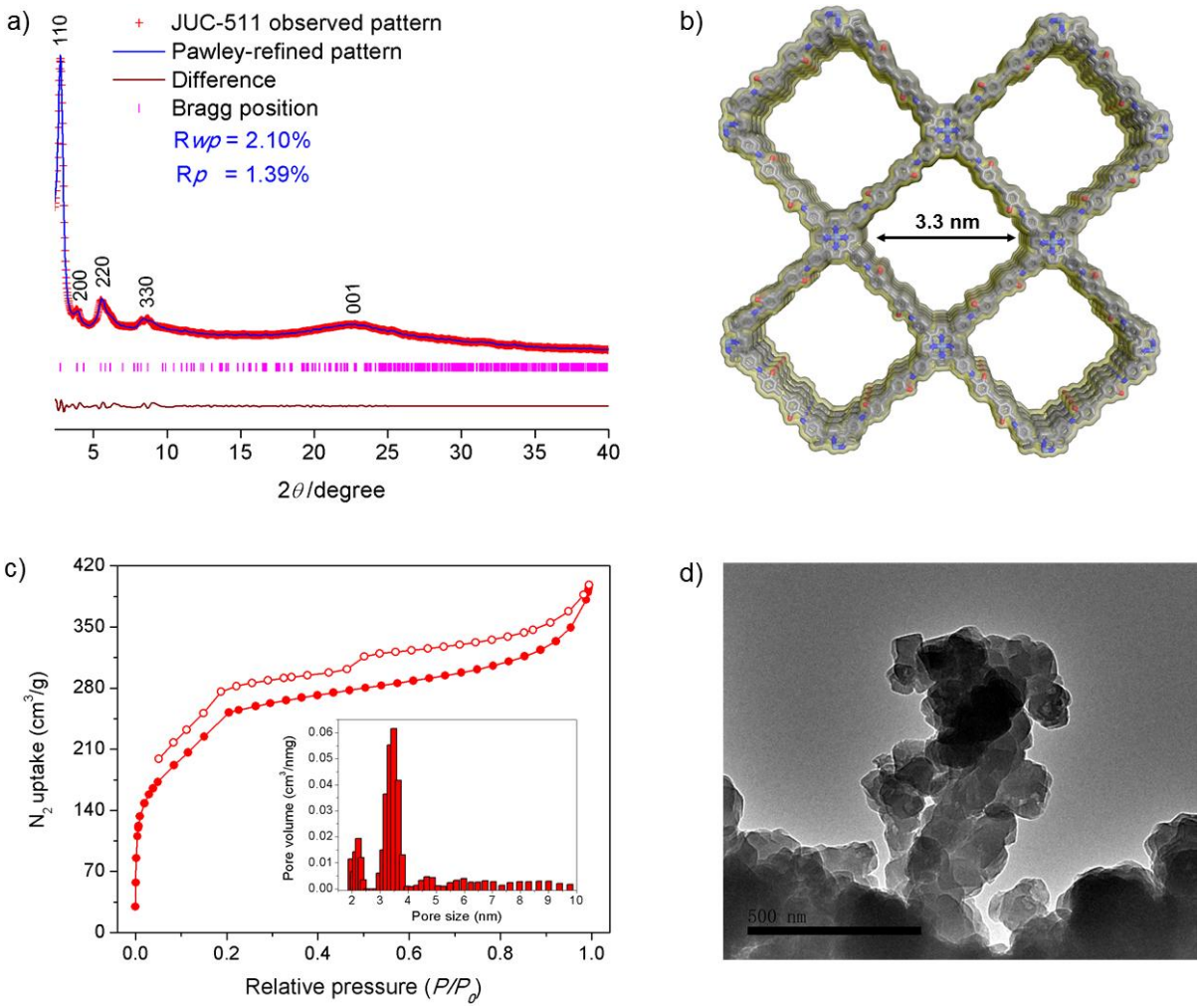

Figure 2. Structural and porosity analyses of JUC-511. a) Pawley refined pattern of JUC-511 based on P_4 space group. b) 3D structural model of JUC-511 with eclipsed layer-stacking structure and predicted 3.3 nm open channel. c) N_2 adsorption-desorption isotherm of JUC-511 with typical two-steps uptake and open-loop hysteresis. Inset, the pore size distribution of JUC-511. d) TEM image of JUC-511 with typical highly aggregated cubic-like structure.

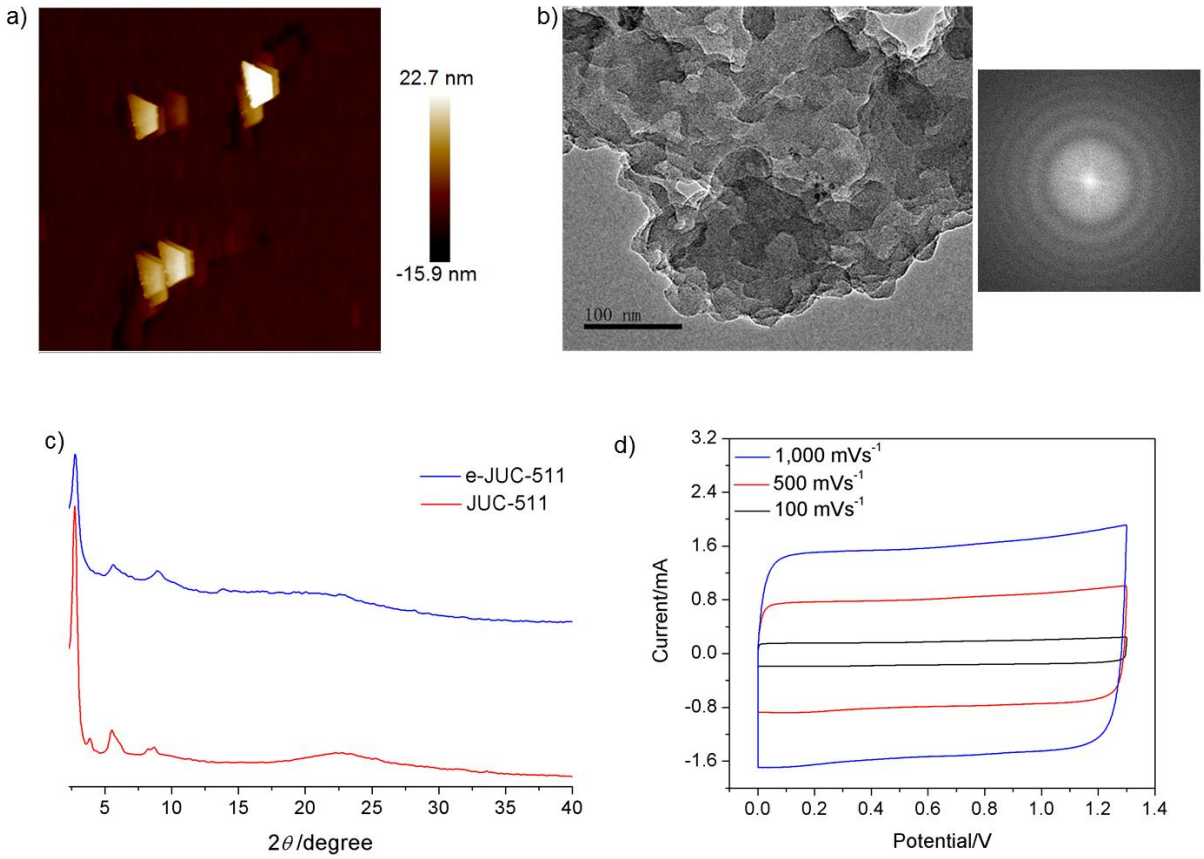

Figure 3. Microstructural and electrochemical analyses of e-JUC-511: a) AFM image of e-JUC-511with maximum layer thickness of ~ 22 nm. b) TEM image of e-JUC-511 with typical exfoliated layer-like structure (left) and the FFT-live capture of certain area of e-JUC-511 under SAED-TEM method (right). c) PXRD patterns of e-JUC-511 and JUC-511. d) CV curves of e-JUC-511 capacitor cell at scan rate of 100 – 1,000 mV s^{-1} with preservation of rectangular in shape.

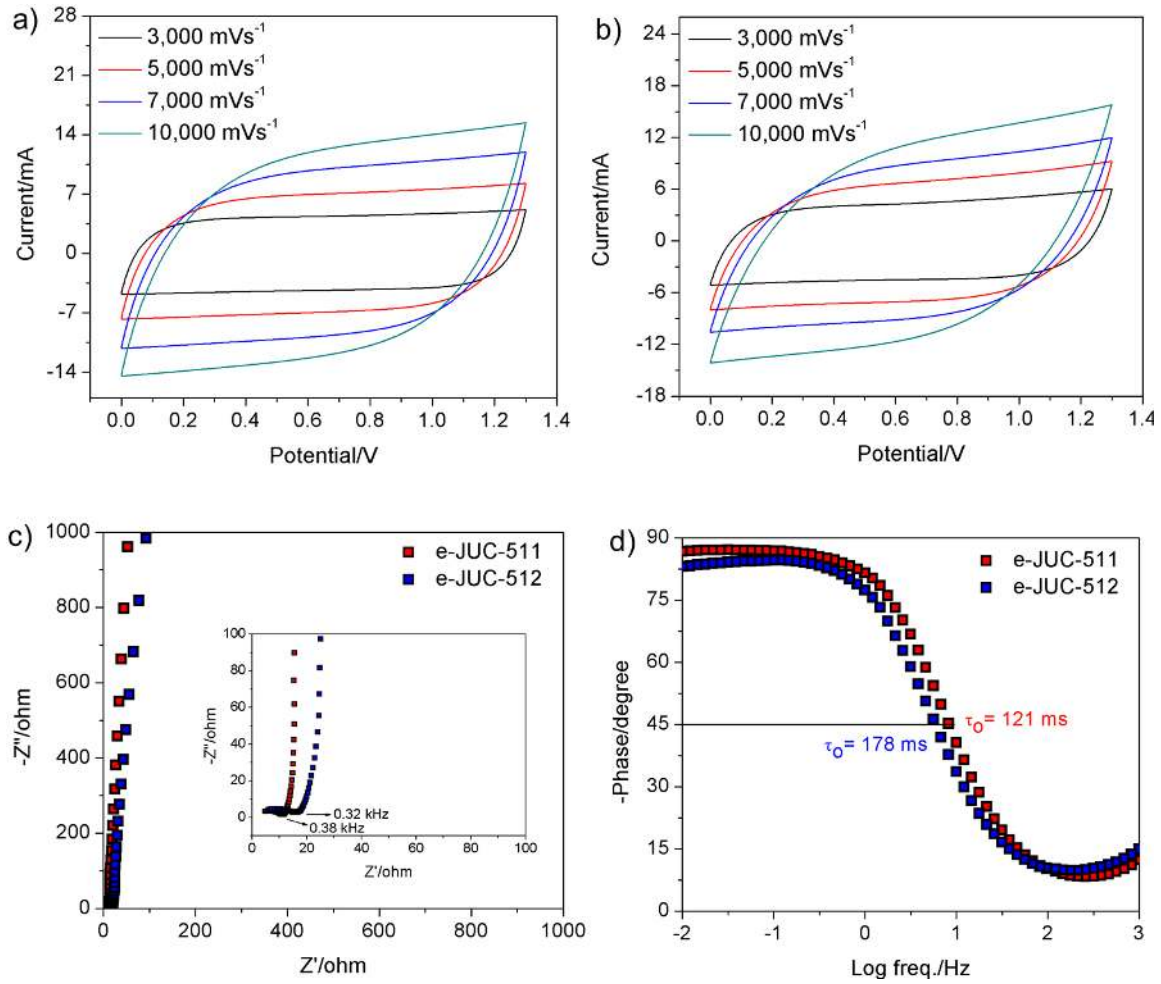

Figure 4. Capacitive performances of e-COF capacitor cells: a) CV curves of e-JUC-511 capacitor cell at scan rate 3,000–10,000 mV s^{-1} with preservation of rectangular shape. b) CV curves of e-JUC-512 capacitor cell at scan rate 3,000–10,000 mV s^{-1} with preservation of rectangular shape. c) Nyquist plot of e-JUC-511 and e-JUC-512 capacitor cells at frequency range 10 mHz–100 kHz and amplitude of 10 mV. d) Bode plot of e-JUC-511 and e-JUC-512 capacitor cells with low τ_0 values.

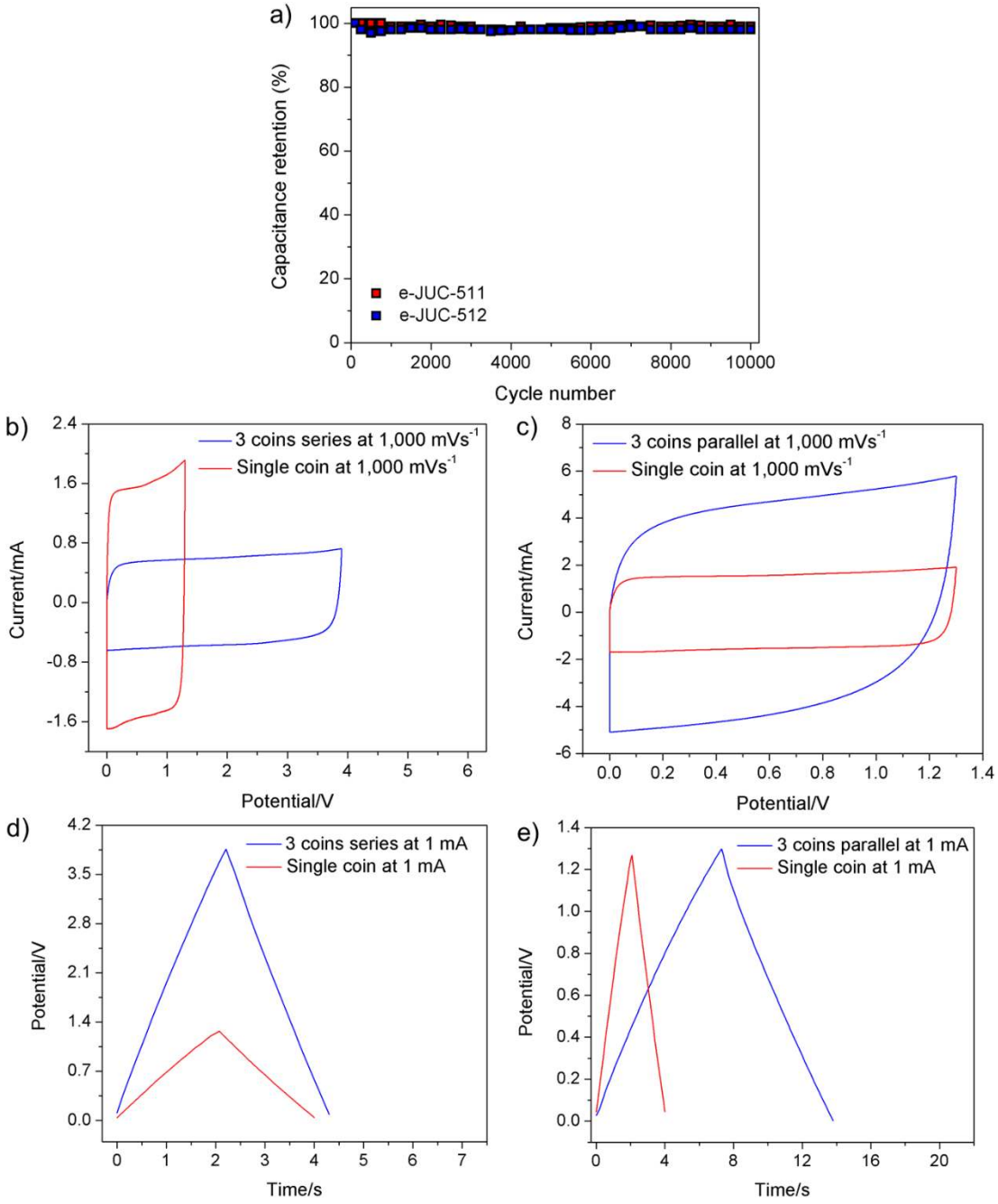

Figure 5. Stability and reliability analyses of e-COF capacitor cells: a) Capacitance retention of e-JUC-511 and e-JUC-512 capacitor cells under 10,000 consecutive cycles. b) CV curves of e-JUC-511 capacitor cell for single and 3 coins assembled in series configuration at 1,000 mV s^{-1}. c) CV curves of e-JUC-511 capacitor cell for single and 3 coins assembled in parallel configuration at 1,000 mV s^{-1}. d) GCD curves of e-JUC-511 capacitor cell for single and 3 coins assembled in series configuration at 1 mA. e) GCD curves of e-JUC-511 capacitor cell for single and 3 coins assembled in parallel configuration at 1 mA.

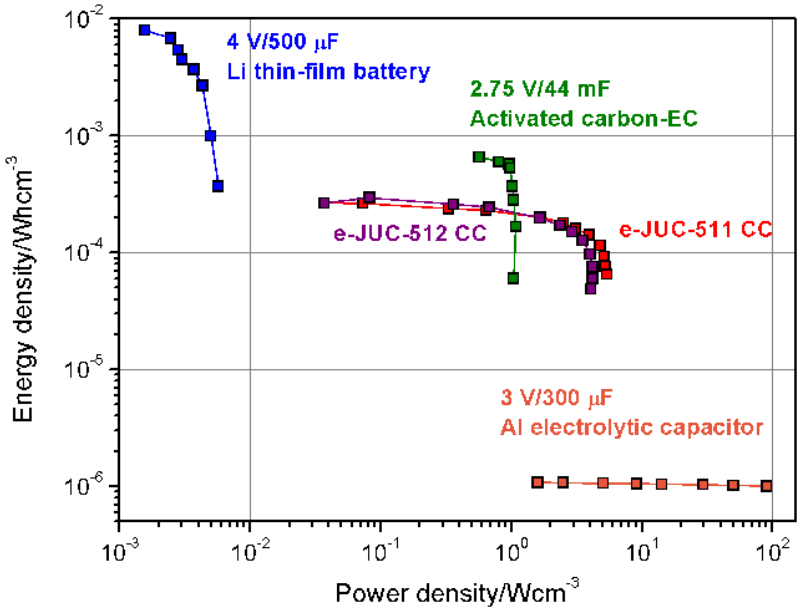

Figure 6. Ragone plot of e-COF capacitor cells where the power density and energy density are calculated based on the total volume of the assembled coin including, micron thickness of the active electrode, current collector and separator as well. Data on Li thin-film battery, commercial AC-EC, and Al electrolytic capacitor are interpolated from ref.[22].

The table of contents entry:

Exfoliated mesoporous 2D COFs (e-COFs) have been prepared and utilized for EDLC electrode construction. The-e-COF capacitor cells perform double-layer charge storage at a high charge-discharge rate (up to 30,000 mVs^{-1}) and exhibit low τ_0 value. The e-COF capacitor cells achieve areal capacitance and gravimetric power that are superior to graphitic-carbon microcapacitors and conventional capacitors and also maintain almost 100% capacitance retention after 10,000 cycles.

Keyword: Covalent organic frameworks, chemical exfoliation, high rate, double-layer capacitor

Y. Yusran, H. Li, X. Guan, D. Li, L. Tang, M. Xue, Z. Zhuang, V. Valtchev, Y. Yan, S. Qiu, and Q. Fang*

Exfoliated Mesoporous 2D Covalent Organic Frameworks for High-Rate Electrochemical Double-Layer Capacitors